Self-Healable, High-Stability Anode for Rechargeable Magnesium Batteries Realized by Graphene-Confined Gallium Metal

Xingwang Zheng, Yuan Yuan,* Dachong Gu, Dajian Li, Ligang Zhang, Liang Wu, Jingfeng Wang, Maximilian Fichtner, and Fusheng Pan

ABSTRACT: In this work, a self-healable, high-stability anode material for rechargeable magnesium batteries (RMBs) has been developed by introducing a core−shell structure of Ga confined by reduced graphene oxide (Ga@rGO). *Via* this Ga@rGO anode, a specific capacity of 150 mAh g^{-1} at a current of 0.5 A g^{-1} stable up to 1200 cycles at room temperature and a specific capacity of 100 mAh g^{-1} under an ultrahigh current of 1 A g^{-1} stable up to 700 cycles at a slightly elevated temperature of 40 °C have been achieved. Additionally, the ultrahigh rate, high-cycling stability, and long-cycle life of the anode are attributed to the stabilized structure; such a low-cost, simple, and environmentally friendly direct drop coating (DDC) method is developed to maximize the original state of the active materials. Remarkably, the self-healing ability of anodes is still presented under the ultrahigh charging current. This anode is promising for the development of high rate and high stability RMBs.

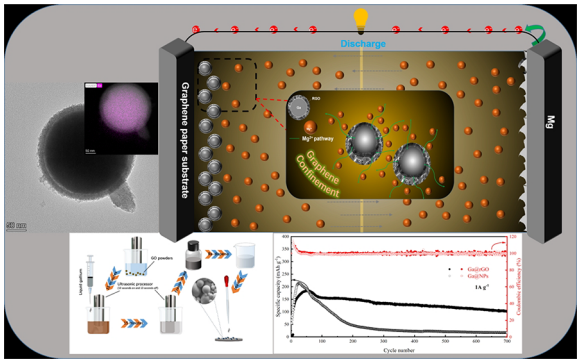

KEYWORDS: *Rechargeable magnesium batteries, anode, self-healing, graphene confinement, electrochemical properties*

The use of renewable energy is inevitable for sustainable development.[1] Rechargeable batteries have been greatly developed in recent years, with the most representative lithium-ion batteries being widely used in electric vehicles, electronic devices, and the grid energy storage field.[2,3] However, lithium-ion batteries have drawbacks such as limited resources and safety, which has lead to the search for a replacement.[4,5] Postlithium-ion batteries with abundant resources of raw materials have been proposed, e.g., sodium (Na), potassium (K), magnesium (Mg), zinc (Zn), and aluminum (Al).[6] Among these alternative batteries, rechargeable magnesium batteries (RMBs) have attracted much attention due to their unique advantages and performance, e.g., high safety, low cost, high-volume capacity, and energy-friendly.[7−9] However, there are still many technology issues that need to be resolved, e.g., the compatibility between electrode materials and electrolytes.[10,11] Cheng et al. reported the construction of heterostructures of CuS and MXene to enhance the conductivity and stability of CuS.[12] Long-cycle stable vanadium−oxygen cathodes were achieved by the intercalation work of crystalline water and magnesium ions on layered V_2O_5 by Xu et al.[13]

Another alternative type of anodes, alloy-type anodes, has been proposed due to their unique advantages, e.g., high compatibility with conventional electrolytes, as reported by Pechberty et al.[14] p-block elements (e.g., Bi, Sn, Sb, In, and Ga) are reported to be able to deliver stable-cycling ability (up to hundreds of cycles), and Mg_xM alloys as anodes for RMBs can be compatible with the noncorrosive simple salt electrolytes.[15] In 2013, Shao et al.[16] reported an experimental capacity of 90 mAh g^{-1} at a current rate of 0.1 C with a full cell of Mg_3Bi_2 anode coupling with the Mo_6S_8 cathode in a 0.4 M $Mg(TFSI)_2$/diglyme electrolyte, where the premagnesiated Bi (Mg_3Bi_2) anode was prepared by assembling Mg//$Mg(BH_4)_2$-$LiBH_4$/diglyme//Bi (nanotube). Another attractive feature for the Mg−Bi anode is the high theoretical volumetric capacity of the Bi−Mg alloy (3783 mAh cm^{-3}) which is comparable to that of the pure Mg anode (3833 mAh cm^{-3}).[17] Another studied alloy element for RMBs is Sn which has a lower alloying voltage and higher theoretical specific capacity compared with Bi. Nanoscale Sn was studied as an anode in RMBs by Singh et al.,[18] and the capacity of 903 mAh g^{-1} has been realized at a low current of 0.002 C. In our previous study, In−Sn−Bi alloys show high cycle stability with capacity retention of 98%,[19] and Bi−Sb−Sn alloys show high specific capacity up to 400 mAh g^{-1}.[20] However, the cycling stability of

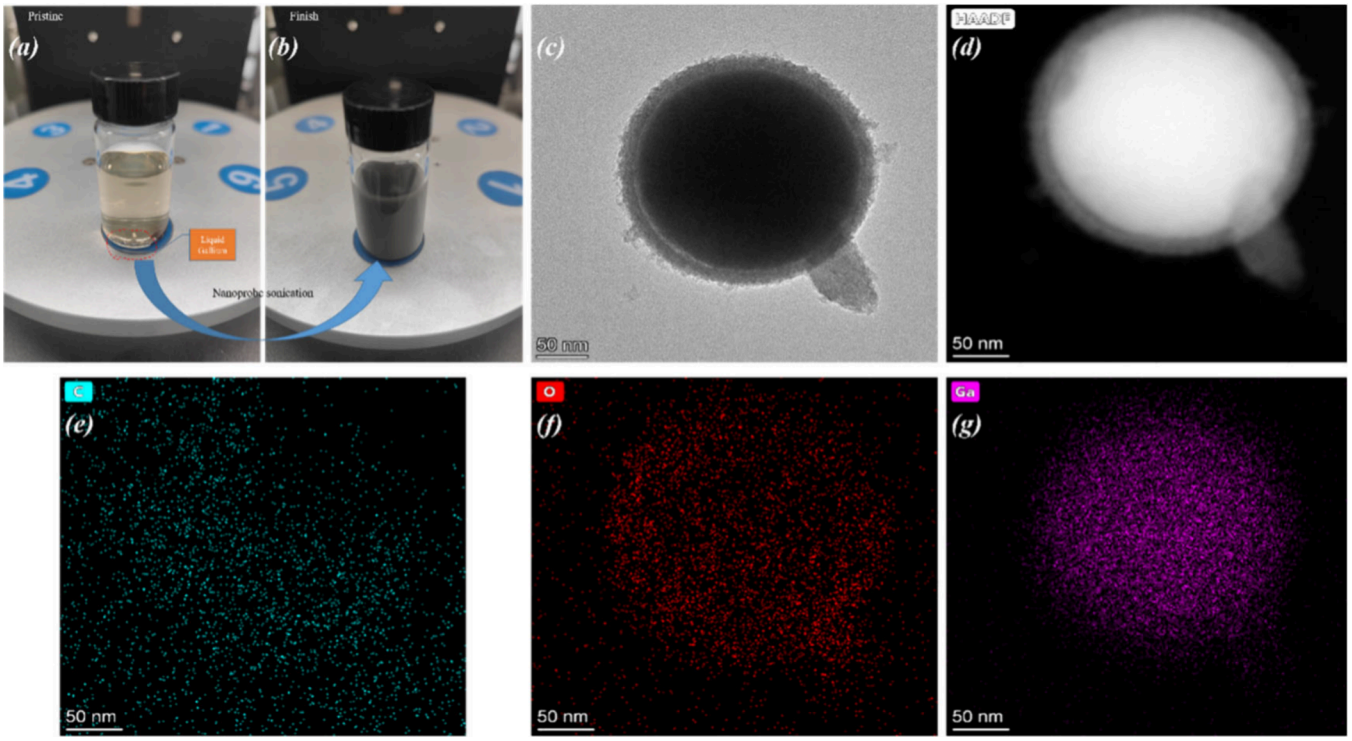

Figure 1. Morphology and elemental distribution of Ga@rGO core−shell structure. (a),(b): Synthesized materials containing liquid Ga and reduced graphene oxide solution before and after sonication. (c),(d): HR-TEM image and HAADF-STEM image of Ga@rGO core−shell particles. (e)−(g): EDS mappings of C, O, and Ga elements.

the above-mentioned anodes is still limited (around one or two hundred cycles followed by fast decaying behavior).

The priority of Ga, compared to other p-block elements, is the nearly room-temperature melting point (29 °C), where the liquid−solid transformation can lead to self-healing ability during the charging/discharging process. Interface modification has also been widely reported as a means of optimizing anodes. For example, the ZnF_2-enriched inorganic/organic SEI layer constructed by Xie et al. avoids the formation of Zn dendrites and hinders the direct contact between the electrolyte and the anode.[21] Gallium-based liquid metals have performed well in alloy anode and interface modification work, and Ga−In−Sn−Zn solid−liquid composites with good adsorption capacity and low Zn-ion mobility energy barriers were prepared by Wang et al.[22,23] Pure Ga metal was first proposed as an anode in galvanic cells by Jahn et al.[24] We have established the cell model of Ga as an anode of RMBs and the calculated electrochemical platform of the Mg−Ga phase transition reaction as 0.2−0.21 V (vs Mg^{2+}/Mg).[25] It is reported by Wang et al.[26] that Mg_2Ga_5 alloy-type anodes can achieve an unprecedented long-cycle life (1000 cycles) at a relatively high (dis)charge rate of 3 C (current density: 922.5 mA g^{-1}), taking advantage of the near-room-temperature solid−liquid phase transformation between Mg_2Ga_5 (solid) and Ga (liquid). This concept opens up new perspectives for the development of anodes for high stability magnesium-ion batteries. Song et al.[27] reported that the wettability of liquid Ga on the stainless steel mesh (SSM) substrate could be significantly enhanced by the construction of a $CuGa_2$ layer on the surface of SSM, and a specific capacity of 225.7 mAh g^{-1} with a current of 100 mA g^{-1} was achieved. The charging/discharging curves of eutectic Ga-based alloys (GaIn, GaSn, GaInSn) and GaInSn were also studied, and a specific capacity of 80 mAh g^{-1} for GaInSn at ∼8 °C was reported.[27] Wei et al.[28] also proposed room-temperature liquid alloys as metal anodes for their corrosive-resistant ability, low nucleation barrier, and uniform ion distribution. The working mechanisms and functions of Ga-based liquid metals as the main working electrodes in primary and secondary batteries have been reviewed by Xing et al.[29]

However, there are still two obstacles that limit the performance of Ga-based anode materials. First, because of the fluidity of Ga in the liquid state, Ga droplet aggregation can occur in the process of demagnetization, which deteriorates the long-life electrochemical performance. Second, Ga would alloy and corrode the metal current collector at room temperature, resulting in the failure of the battery. In this work, a self-healable, high-stability, and noncorrosive anode material compatible with conventional electrolyte containing Cl^- for RMBs has been developed by using the graphene confining the gallium (Ga) metal (Ga@rGO). First, the developed "core−shell structure (Ga@rGO)" can prevent Ga from agglomeration, stabilize the structure, and make the anode self-healable during the liquid−solid transformation. Second, the rGO shell can also isolate the Ga and the metal current collector to avoid the corrosion. In addition, the concept of the preparation of graphene confining anode materials by the direct drop coating (DDC) method is also proposed in this work to maximize the integrity of the core−shell structure. The performance of gallium nanoparticles (Ga-NPs) as anodes was also studied for comparison. The gallium nanoparticles and Ga@rGO were produced by a simple, one-pot nanoprobe sonication method, reported by Zhang et al.[30]

The synthesized materials of Ga@rGO were characterized using scanning transmission electron microscopy (STEM) as shown in Figure 1, and the desired core−shell structure was

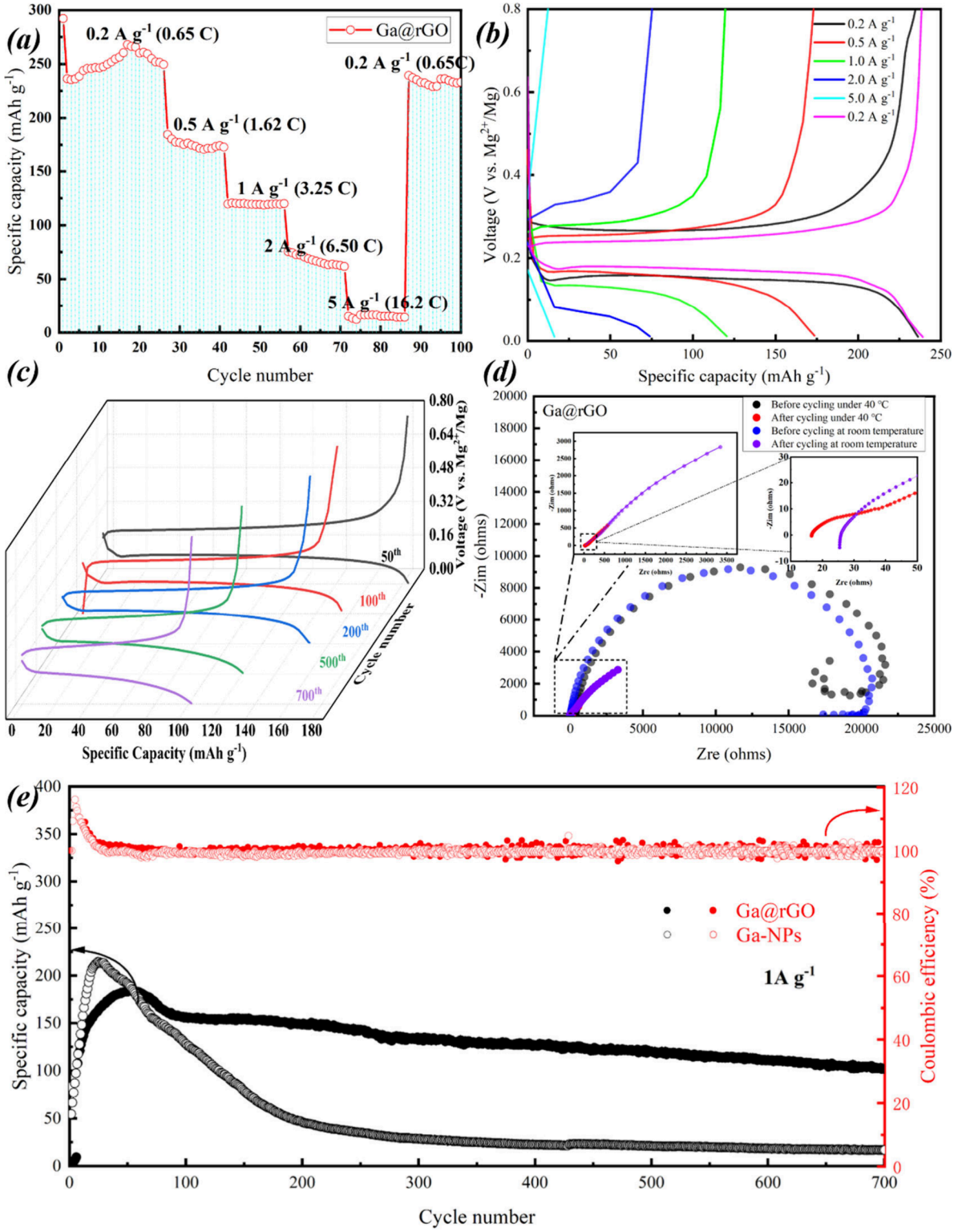

Figure 2. Electrochemical properties: (a) rate capability of Ga@rGO with the current density between 0.5 A g^{-1} and 5 A g^{-1}; (b) charging/discharging curves of Ga@rGO under different current densities; (c) selected charging/discharging curves of the 50th, 100th, 200th, 500th, and 700th cycles at 40 °C with a current of 1 A g^{-1}; (d) Nyquist plots of Ga@rGO; (e) cycling capability (solid black circles) and Coulombic efficiency (solid red circles) of Ga@rGO and cycling capability (open black circles) and Coulombic efficiency (open red circles) of Ga-NPs at a current of 1 A g^{-1} at 40 °C.

perfectly achieved. To avoid formatting (GaO)OH from the reaction between Ga and H_2O,[31] ethanol was considered as a solvent in the synthetic procedure. The high-resolution transmission electron microscopy (HR-TEM) and high-angle annular dark field (HAADF) images of the Ga@rGO are shown in Figure 1(c) and Figure 1(d), where the core−shell structure is clearly observed. The Ga particles (in perfect sphere state) are surrounded by reduced graphene oxide

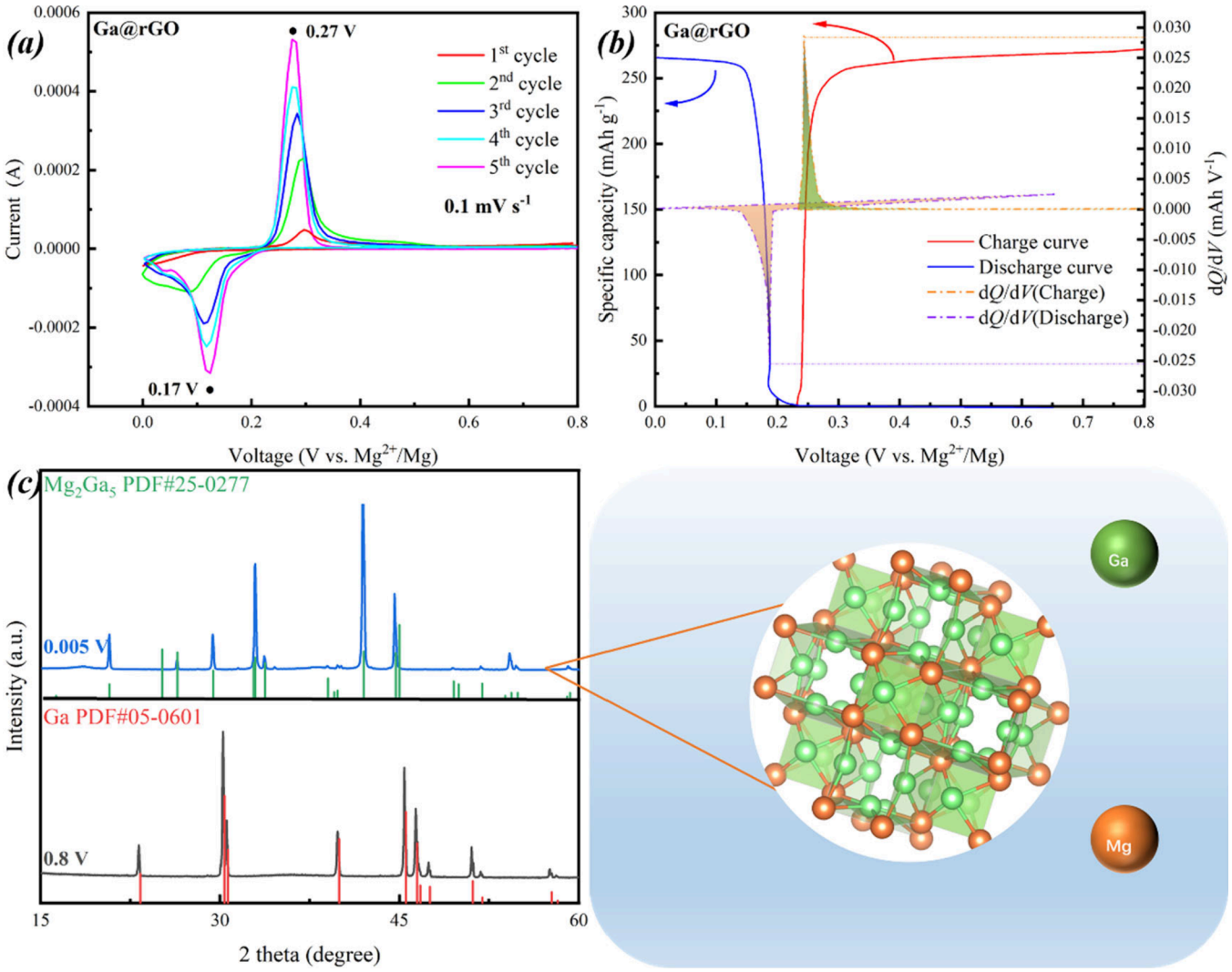

Figure 3. (a) Typical cyclic voltammetric curves of Ga@rGO electrode carried out at the scan rate of 0.1 mV s^{-1}; (b) charge and discharge curves of Ga@rGO and its corresponding dQ/dV curves; and (c) *ex-situ* XRD patterns of Ga@rGO and atomic structure model of Mg_2Ga_5.

(rGO), and the thickness of shell is in a × 10 nm scale. The X-ray photoelectron spectroscopy (XPS) characterization also shows that Ga is concentrated to form the core, and a layer of O totally covers the Ga sphere, where a little larger wafer of the O distribution is presented compared to the distribution of Ga. Because of the background of the carbon substrate, a wide distribution of C elements is presented. As shown in Figure 1(f), there is a thin layer of O around the Ga particle. One possible source is that during the preparation process Ga may react with oxygen in the air and form an oxide layer such as Ga_2O_3. Another source could be coming from the remaining unreduced GO.

Using the synthesized Ga@rGO and Ga-NPs, the electrodes were fabricated by direct drop coating (DDC) of active materials on the graphite paper substrate, where the active materials' mass loading can be easily controlled within a range of 1−2 mg. These half-cells were processed at the temperature of 40 °C, as shown in Figure 2(e), and the reference experiment using Ga@rGO at room temperature of 25 °C is shown in Figure S4(a) of the Supporting Information. It should be noted that the mass fraction of rGO in the prepared Ga@rGO is less than 1 wt %, and recent studies have shown that pure rGO does not provide storage capacity for Mg.[32] Hence, the storage capacity of rGO was not taken into consideration. As shown in Figure 2(a),(b), fast charging/discharging performance has been realized through Ga@rGO anode material, where the insertion and extraction of Mg^{2+} at a high current of 5 A g^{-1} was achieved. In the rate test, the specific capacities of around 250, 175, 125, 70, and 15 mAh g^{-1} with the current of 0.2 A g^{-1} (0.62 C), 0.5 A g^{-1} (1.62 C), 1 A g^{-1} (3.25 C), 2 A g^{-1} (6.5 C), and 5 A g^{-1} (16.2 C), respectively, have been presented for anode Ga@rGO. As the rate went back to the initial 0.2 A g^{-1}, a large reversible capacity of about 250 mAh g^{-1} was presented again for the Ga@rGO electrode, indicating the good reversibility of redox reactions from high rates to low rates. Remarkably, for Ga@rGO electrodes processed at 40 °C, a specific capacity of 100 mAh g^{-1} under an ultrahigh current of 1 A g^{-1} was stabilized up to 700 cycles, as shown in Figure 2(e) and Figure 2(c). According to Figure S4(a), with a little lower current of 0.5 A g^{-1}, Ga@rGO can even charge/discharge smoothly at room temperature with a specific capacity of around 150 mAh g^{-1} and an ultralong cycle life of 1200 times, indicating the high stability of Ga@rGO during the cycling process. Under a current of 0.2 A g^{-1}, a stable high specific capacity of more than 250 mAh g^{-1} has been achieved (Figure S4(b)).

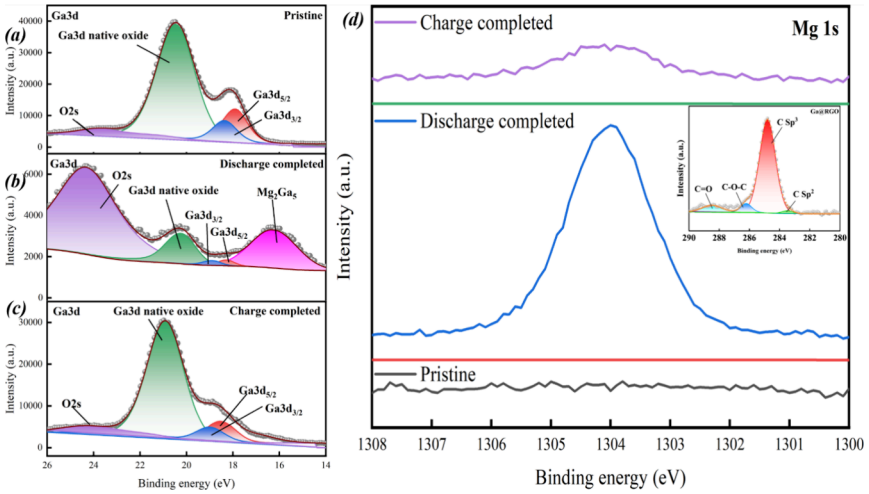

Figure 4. X-ray photoelectron spectroscopy and the corresponding peak analysis of Ga and Mg elements in different electrochemical states: (a) pristine state of Ga@rGO; (b) discharge to 0.005 V of Ga@rGO; (c) charge to 0.8 V of Ga@rGO; and (d) entire change process of the Mg element (the subfigure is XPS results of rGO).

Additionally, as shown in Figure 2(e), with the processing temperature of 40 °C, Ga@rGO shows much better electrochemical performance than Ga-NPs, with higher specific capacity and better cycling stability, which indicates the good self-healing feature attributed by the effective confining function coming from the rGO shell. As can be seen from Figure S9, after cycling, the active material of Ga-NPs obviously was agglomerated, which means Ga-NPs can exhibit a considerable specific capacity in a short period of cycling, but the specific capacity decreases fast.

It can be clearly seen in Figure2(b) that the smaller the current density, the smaller the polarization−voltage. This can be attributed to the fact that ion conduction lags behind electron conduction. When the current density increases, the electron conduction is faster, which leads to more serious ion hysteresis and then shows greater polarization−voltage.

The conductivity is inversely proportional to the resistance. In Figure 2(d), the impedance of the Ga@rGO anode material before cycling is almost the same as that after cycling at room temperature. Meanwhile, the impedance spectrum shows a large semicircular shape without a Warburg impedance, which indicates that the conductivity of the electrode before and after cycling at room temperature is unchanged and shows low diffusion. Before and after cycling, the impedance of the Ga@rGO anode material decreases significantly at 40 °C. The Warburg impedance is observed, and the conductivity of the Ga@rGO anode material is achieved and can be enhanced by cycling at 40 °C.

To clarify the mechanism of Mg^{2+} reacting with Ga@rGO, the cyclic voltammogram and phase transformation information has been shown in Figure 3. The phase transformation process of Ga@rGO in the charging/discharging process under a current of 1 A g^{-1} was characterized using *ex-situ* XRD analysis. Two positions were chosen for the *ex-situ* XRD analysis: one was the position of discharging completed (at 0.005 V), and the other was that of charging completed (at 0.8 V).

According to Figure 3(a), there is only one peak in the charging/discharging process, corresponding to the formation of a Mg−Ga compound at around 0.17 V in the charging process and the decomposition of a Mg−Ga compound at around 0.27 V in the discharging process, respectively. These two potentials are consistent with the potentials of charge and discharge voltage platforms as shown in Figure 3(b). During the electrochemical process, the differential capacity curve dQ/dV in Figure 3(b) reveals the initial and final range of reaction voltages at around 0.15−0.3 V.

The *ex-situ* XPS characterization was used to investigate the specific electronic orbit changes of Mg and Ga during the magnesiation/demagnesiation process. The detailed valence changes of Ga and Mg are shown in Figure 4(a)−(d). As shown in Figure 4(d), the intensity of functional group peaks, e.g., C═O and C−O, in rGO is much smaller than those in GO (as shown in ref 30), which indicates that rGO has been successfully obtained and there is still a small amount of GO. During the transformation of GO to rGO, the metal Ga has a reducing effect and contributes to the deoxidation of GO due to its negative standard electrode potential. At the same time, the introduction of hydrogen ions in the material synthesis removes the natural oxide layer formed on the surface after Ga reduction. It is not yet possible to quantitatively describe the extent of graphene oxide reduction, but by comparing the oxygen content with that of graphene oxide, we confirm that most GO has achieved the rGO transition. This transition allows Ga to be freed from GaO, and comparison samples without the addition of hydrochloric acid would make Ga fully oxidized,[30] which is detrimental to the reaction of Ga with Mg.

As for the intensity change of the Ga element shown in Figure 4(a)−(c), it is related to the insertion and dissolution of Mg in a complete cycle. During the characterization process, pure Ga is oxidized, and Ga_2O_3 is formed. Hence the peaks of O 2s are observed in the XPS results. In this study, the morphology of the reduced graphene oxide did not change before and after cycling, which indicates the oxygen presented in XPS results came from the surface layer Ga_2O_3 and did not participate in the reaction. It is necessary to mention that the relative intensities of O 2s, as shown in Figure 4(a)−(c), are close to each other, and the values are all around 7000 (arbitrary unit). In the discharging process, Mg ions are combined with metallic Ga to form Mg−Ga compounds (Figure 4(b)). In the charging process, Mg_2Ga_5 is dealloyed, and the pure Ga is reformed (Figure 4(c). It should be noted, here, that the *ex-situ* XPS has been employed, and the sample was oxidized immediately when taking it out of the cell;

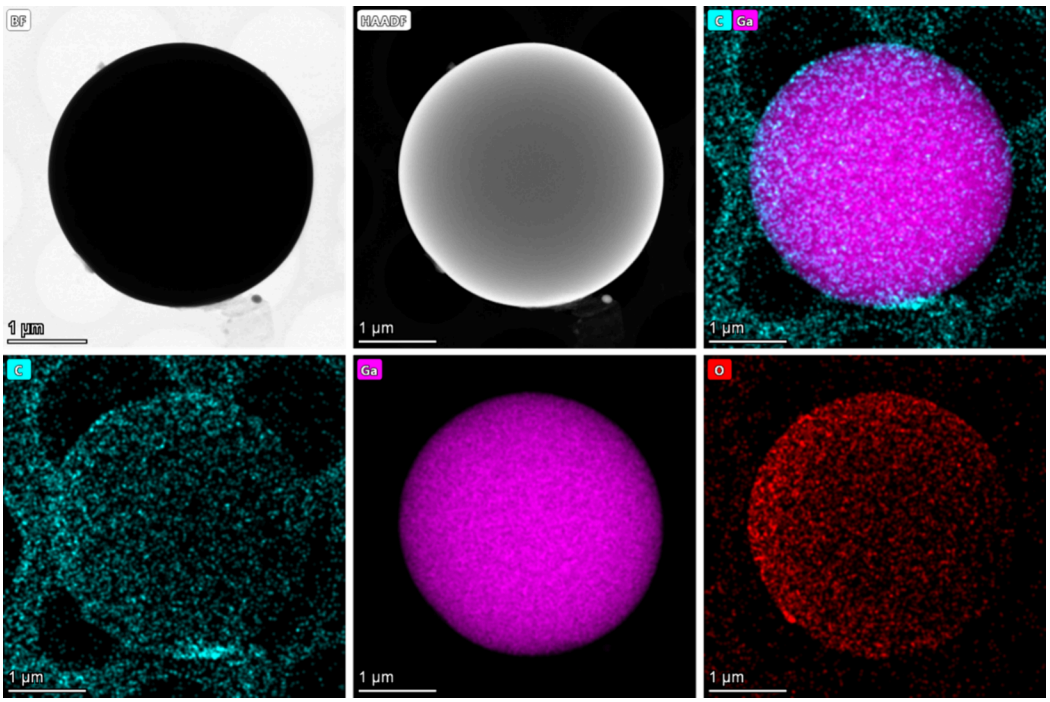

Figure 5. TEM images and corresponding EDS mapping of the Ga@rGO anode of 0.8 V after the charging process.

therefore, most of Ga were in the oxidation state, as shown in Figure 4(c). In the process, Mg metal is also oxidized into a Mg ion, which corresponds to the positive divalent oxidation state, as shown in Figure 4(d).

As for the XPS analysis of the Mg−Ga system from the initial position to the position of charge completed, binding energies of Ga $3d_{5/2}$ and Ga $3d_{3/2}$ at 18.53 and 18.99 eV, respectively, stand for the binding energies of pure Ga, and the intensity of the peak at 20.86 eV in Figure 4(b) indicates the formation of the Mg−Ga bond of Mg_2Ga_5.

Ex-situ TEM images of Ga@rGO after the charging process have been shown in Figure 5. It can be seen that the Ga particle remains spherical after cycling, and the rGO layer is still attached to the surface of the Ga particle with a thinner thickness, compared with that shown in Figure 1. In addition, according to the EDS mapping, the distributions of oxygen and carbon are still in a quite perfect sphere shape, very concentrated around the Ga sphere. As can be seen in Figure 5, the Ga particles are still in the shape of nanospheres after cyclic charging, and the rGO layer is still attached to the surface of Ga particles; however, compared with that before the cycling (Figure 1), its thickness is significantly thinner and almost invisible to the naked eye. However, from the EDS spectra, it can still be observed that the C element, representing rGO, uniformly covers the surface of the anode material.

To conclude, the morphology and structure of the active particles are highly stabilized, retaining the original morphology before and after cycling with a slight increase in size. The phenomenon just mentioned about the size increase may be related to its specific capacity attenuation.

As shown in Figure 5 (the TEM images of Ga@rGO after charging is completed), the sizes of the particles of Ga@rGO are generally larger, but with small increments, than those of particles shown in Figure 1 (the TEM images of Ga@rGO original particles). Combining Figure 1 and Figure 5, it is revealed that, with rGO confining and stabilizing the structure, Ga@rGO exhibits excellent self-healing capability during the cycling process. The DDC method also contributes to the perfectly maintained Ga@rGO core−shell nanostructure. It can been seen, as shown in Figure S8, that the Ga particles using the conventional composite slurry preparation method are ellipsoidal; in addition, they are larger and more uneven than that using the DDC method.

As shown in the charging/discharging tests of Figure 2(e) and cyclic voltammetry curves of Figure 3(a), there are activation stages in the initial few cycles, which may be attributed to the configuration rearrangement of active materials and SEI. In addition, it is seen that the specific capacities of Ga-NPs are larger than those of Ga@rGO during the first 60 cycles, which can be attributed to the instant contact between Mg and Ga in Ga-NPs. However, with the cycling process, Ga particles agglomerate, resulting in accelerated specific capacity attenuation, and for Ga@rGO, the existence of the rGO layer maintains the core−shell structure of Ga@rGO.

In general, the initial charge−discharge curve of a battery is quite different from that of the subsequent curves of the battery. It is generally believed the main reason is that most of the active materials in the electrodes will be rearranged during the first several cycles, and the microstructure will approach a stable state. After self-arrangement, the most favorable electrochemical state for charging and discharging will be achieved. However, in this work, the first complete charging/discharging curve of Ga@rGO is not much different from that after stabilization, and the liquid state of Ga at 40 °C is close to the stable electrochemical state. Then, it can be proposed that the battery involving the solid−liquid phase transformation has special states changes during the charge−discharge process.

With respect to the active materials, it is shown that the Ga@rGO shows better electrochemical performance than the Ga-NPs electrode, both using the DDC method for the coating

on the current collectors, which can be attributed to the self-healing ability of Ga@rGO. The continuous decay of specific capacity of Ga-NPs is attributed to the decrease of specific surface area because of the agglomeration. Additionally, for Ga-NPs, the bare naked liquid Ga can corrode the metal current collectors, resulting in the electrochemical performance decaying and even a cell short circuit failure. It should be noted that the battery using the conventional composite slurry coating method for the electrode does not show capacity at room temperature. Here, the battery using the same active materials coating by the DDC method shows a capacity more than 150 mAh g^{-1}. Additionally, the simple, cost-effective, and environmentally friendly DDC method shows its advance of maximizing the original microstructure of electrode materials.

In this work, a self-healable, ultrahigh rate, and long-cycle-life anode material for RMBs has been developed by introducing a core−shell structure of Ga confined by reduced graphene oxide (Ga@rGO). The excellent electrochemical performance can be attributed to 1) a core−shell structure with the effect of rGO confining and 2) the DDC method. The coated reduced graphene oxide around Ga can perfectly protect Ga from agglomerating, and after cycling, the rGO layer is helpful for Ga@rGO to keep the original core−shell structure stable. A long-cycle life of Ga@rGO with a specific capacity of more than 100 mAh g^{-1} under an ultrahigh current density of 1 A g^{-1} (3.25 C) has been realized. Additionally, the electrochemical activation of Ga in Ga@rGO at room temperature has been realized with a specific capacity of over 150 mAh g^{-1} at a current density of 0.5 A g^{-1}, and an ultralong cycle life exceeded 1200 cycles. The ultralong cycle life at room temperature and the long cycle life at 40 °C of Ga@rGO were realized by the developed direct drop coating method.

The combination of reduced graphene oxide confinement, liquid self-healing metal, core−shell structure, and DDC method provides a new design strategy for high-rate and long-cycle-life anodes of RMBs.

ASSOCIATED CONTENT

Data Availability Statement

The raw/processed data required to reproduce these findings are available on request.

AUTHOR INFORMATION

Corresponding Author

Yuan Yuan − *National Engineering Research Center for Magnesium Alloys, College of Materials Science and Engineering, Chongqing University, 400044 Chongqing, China; School of Materials Science and Engineering, Central South University, 410083 Changsha, China; Chongqing Institute of New Energy Storage Materials and Equipment, 401122 Chongqing, China;* orcid.org/0000-0002-6883-199X; Email: yuanyuan17@cqu.edu.cn, yuan.yuan.er@gmail.com

Authors

Xingwang Zheng − *National Engineering Research Center for Magnesium Alloys, College of Materials Science and Engineering, Chongqing University, 400044 Chongqing, China*

Dachong Gu − *National Engineering Research Center for Magnesium Alloys, College of Materials Science and Engineering, Chongqing University, 400044 Chongqing, China*

Dajian Li − *National Engineering Research Center for Magnesium Alloys, College of Materials Science and Engineering, Chongqing University, 400044 Chongqing, China;* orcid.org/0000-0001-9057-6377

Ligang Zhang − *School of Materials Science and Engineering, Central South University, 410083 Changsha, China*

Liang Wu − *National Engineering Research Center for Magnesium Alloys, College of Materials Science and Engineering, Chongqing University, 400044 Chongqing, China; Chongqing Institute of New Energy Storage Materials and Equipment, 401122 Chongqing, China;* orcid.org/0000-0002-9988-8593

Jingfeng Wang − *National Engineering Research Center for Magnesium Alloys, College of Materials Science and Engineering, Chongqing University, 400044 Chongqing, China; Chongqing Institute of New Energy Storage Materials and Equipment, 401122 Chongqing, China*

Maximilian Fichtner − *Helmholtz Institute Ulm (HIU) Electrochemical Energy Storage, D-89081 Ulm, Germany; Institute of Nanotechnology (INT), Karlsruhe Institute of Technology (KIT), D-76021 Karlsruhe, Germany;* orcid.org/0000-0002-7127-1823

Fusheng Pan − *National Engineering Research Center for Magnesium Alloys, College of Materials Science and Engineering, Chongqing University, 400044 Chongqing, China; Chongqing Institute of New Energy Storage Materials and Equipment, 401122 Chongqing, China*

Author Contributions

Xingwang Zheng: Writing—original draft, Methodology, Investigation, Data curation, Formal analysis, Validation. **Yuan Yuan:** Supervision, Project administration, Funding acquisition, Conceptualization, Resources, Writing—review and editing. **Dajian Li:** Conceptualization, Methodology, Visualization, Writing—review and editing. **Dachong Gu:** Investigation, Visualization. **Liang Wu:** Resources, Writing—review and editing. **Ligang Zhang:** Resources. **Jingfeng Wang:** Resources. **Maximilian Fichtner:** Writing—review and editing. **Fusheng Pan:** Supervision, Project administration, Funding acquisition.

Notes

The authors declare no competing financial interest.

ACKNOWLEDGMENTS

This work is financially supported by the National Key R&D Program of China (2023YFB3809500) and National Natural Science Foundation of China (U23A20555).

REFERENCES

(1) Goodenough, J. B.; Park, K. S. The Li-Ion Rechargeable Battery: A Perspective. *J. Am. Chem. Soc.* **2013**, *135* (4), 1167−1176.

(2) Dunn, B.; Kamath, H.; Tarascon, J. M. Electrical Energy Storage for the Grid: A Battery of Choices. *Science* **2011**, *334* (6058), 928−935.

(3) Goodenough, J. B. Electrochemical energy storage in a sustainable modern society. *Energy Environ. Sci.* **2014**, *7* (1), 14−18.

(4) Manthiram, A. Electrical energy storage: Materials challenges and prospects. *MRS Bull.* **2016**, *41* (08), 624−631.

(5) Yang, Y.; Xiong, X. M.; Chen, J.; Peng, X. D.; Chen, D. L.; Pan, F. S. Research advances of magnesium and magnesium alloys worldwide in 2022. *J. Magnesium Alloys* **2023**, *11* (8), 2611−2654.

(6) Foundations for the future. *Nat. Energy* **2016**, DOI: 10.1038/Nenergy16147.

(7) Su, S.; Huang, Z.; NuLi, Y.; Tuerxun, F.; Yang, J.; Wang, J. A novel rechargeable battery with a magnesium anode, a titanium dioxide cathode, and a magnesium borohydride/tetraglyme electrolyte. *Chem. Commun.* **2015**, *51* (13), 2641−2644.

(8) Carter, T. J.; Mohtadi, R.; Arthur, T. S.; Mizuno, F.; Zhang, R.; Shirai, S.; Kampf, J. W. Boron Clusters as Highly Stable Magnesium-Battery Electrolytes. *Angew. Chem., Int. Ed.* **2014**, *53* (12), 3173−3177.

(9) Doe, R. E.; Han, R.; Hwang, J.; Gmitter, A. J.; Shterenberg, I.; Yoo, H. D.; Pour, N.; Aurbach, D. Novel, electrolyte solutions comprising fully inorganic salts with high anodic stability for rechargeable magnesium batteries. *Chem. Commun.* **2014**, *50* (2), 243−245.

(10) Li, Z. Y.; Hacker, J.; Fichtner, M.; Zhao-Karger, Z. Cathode Materials and Chemistries for Magnesium Batteries: Challenges and Opportunities. *Adv. Energy Mater.* **2023**, DOI: 10.1002/aenm.202300682.

(11) Li, D. J.; Yuan, Y.; Liu, J. W.; Fichtner, M.; Pan, F. S. A review on current anode materials for rechargeable Mg batteries. *J. Magnesium Alloys* **2020**, *8* (4), 963−979.

(12) Cheng, Z.; Xu, Y. A.; Zhang, X. D.; Peng, Q. F.; Wang, K.; Zhang, X.; Sun, X. Z.; An, Q. Y.; Mai, L. Q.; Ma, Y. W. An interfacial covalent bonding coupled ultrafine CuS-nanocrystals/MXene heterostructure for efficient and durable magnesium storage. *Journal of Materials Chemistry A* **2023**, *11* (23), 12176−12184.

(13) Xu, Y. N.; Deng, X. W.; Li, Q. D.; Zhang, G. B.; Xiong, F. Y.; Tan, S. S.; Wei, Q. L.; Lu, J.; Li, J. T.; An, Q. Y.; et al. Vanadium Oxide Pillared by Interlayer Mg < SUP > 2+</SUP> Ions and Water as Ultralong-Life Cathodes for Magnesium-Ion Batteries. *Chem.* **2019**, *5* (5), 1194−1209.

(14) Pechberty, C.; Hagopian, A.; Ledeuil, J. B.; Foix, D.; Allouche, J.; Chotard, J. N.; Luzanin, O.; Bitenc, J.; Dominko, R.; Dedryvere, R.; et al. Alloying electrode coatings towards better magnesium batteries. *Journal of Materials Chemistry A* **2022**, *10* (22), 12104−12113.

(15) Zhao, Y. M.; Du, A. B.; Dong, S. M.; Jiang, F.; Guo, Z. Y.; Ge, X. S.; Qu, X. L.; Zhou, X. H.; Cui, G. L. A Bismuth-Based Protective Layer for Magnesium Metal Anode in Noncorrosive Electrolytes. *Acs Energy Letters* **2021**, *6* (7), 2594−2601.

(16) Shao, Y.; Gu, M.; Li, X.; Nie, Z.; Zuo, P.; Li, G.; Liu, T.; Xiao, J.; Cheng, Y.; Wang, C.; et al. Highly Reversible Mg Insertion in Nanostructured Bi for Mg Ion Batteries. *Nano Lett.* **2014**, *14* (1), 255−260.

(17) Kravchyk, K. V.; Piveteau, L.; Caputo, R.; He, M.; Stadie, N. P.; Bodnarchuk, M. I.; Lechner, R. T.; Kovalenko, M. V. Colloidal Bismuth Nanocrystals as a Model Anode Material for Rechargeable Mg-Ion Batteries: Atomistic and Mesoscale Insights. *ACS Nano* **2018**, *12* (8), 8297−8307.

(18) Singh, N.; Arthur, T. S.; Ling, C.; Matsui, M.; Mizuno, F. A high energy-density tin anode for rechargeable magnesium-ion batteries. *Chem. Commun.* **2013**, *49* (2), 149−151.

(19) Zheng, X.; Song, C.; Yuan, Y.; Li, D.; Gu, D.; Wu, L.; Huang, G.; Wang, J.; Pan, F. High stability In−Sn−Bi multi-element alloy anode for Mg ion batteries. *J. Power Sources* **2023**, *575*, 233141.

(20) Liu, F.; Cao, G.; Ban, J.; Lei, H.; Zhang, Y.; Shao, G.; Zhou, A.; Fan, L. Recent advances based on Mg anodes and their interfacial modulation in Mg batteries. *Journal of Magnesium and Alloys* **2022**, *10*, 2699−2716.

(21) Xie, D.; Sang, Y.; Wang, D. H.; Diao, W. Y.; Tao, F. Y.; Liu, C.; Wang, J. W.; Sun, H. Z.; Zhang, J. P.; Wu, X. L. ZnF < sub > 2</sub>-Riched Inorganic/Organic Hybrid SEI: in situ-Chemical Construction and Performance-Improving Mechanism for Aqueous Zinc-ion Batteries. *Angew. Chem., Int. Ed.* **2023**, DOI: 10.1002/anie.202216934.

(22) Wang, W.; Zuo, P. J.; Yin, G. P.; Du, C. Y.; Huo, H.; Ma, Y. L.; Gao, Y. Z. A dendrite-free Ga-In-Sn-Zn solid-liquid composite anode for rechargeable zinc batteries. *Energy Storage Materials* **2023**, *58*, 195−203.

(23) Wei, C. L.; Tan, L. W.; Zhang, Y. C.; Wang, Z. R.; Xi, B. J.; Xiong, S. L.; Feng, J. K. Interfacial engineering on metal anodes in rechargeable batteries. *Energychem* **2022**, *4* (5), 100089.

(24) Jahn, D.; Plust, H. G. Possible Use of Gallium as Negative Electrode in Galvanic Cells. *Nature* **1963**, *199* (489), 806.

(25) Song, C.; Yuan, Y.; Gu, D. C.; Chen, T.; Liu, Y. P.; Tang, A. T.; Wu, L.; Li, D. J.; Pan, F. S. The Evaluation of Mg-Ga Compounds as Electrode Materials for Mg-Ion Batteries via Ab Initio Simulation. *J. Electrochem. Soc.* **2021**, *168* (11), 110539.

(26) Wang, L.; Welborn, S. S.; Kumar, H.; Li, M. N.; Wang, Z. Y.; Shenoy, V. B. High-Rate and Long Cycle-Life Alloy-Type Magnesium-Ion Battery Anode Enabled Through (De)-magnesiation-Induced Near-Room-Temperature Solid-Liquid Phase Transformation. *Adv. Energy Mater.* **2019**, *9* (45), 201902086.

(27) Song, M. J.; Niu, J. Z.; Cui, W. R.; Bai, Q. G.; Zhang, Z. H. Self-healing liquid Ga-based anodes with regulated wetting and working temperatures for advanced Mg ion batteries. *Journal of Materials Chemistry A* **2021**, *9* (31), 17019−17029.

(28) Wei, C. L.; Tan, L. W.; Zhang, Y. C.; Wang, Z. R.; Xi, B. J.; Xiong, S. L.; Feng, J. K.; Qian, Y. T. Review of room-temperature liquid metals for advanced metal anodes in rechargeable batteries. *Energy Storage Mater.* **2022**, *50*, 473−494.

(29) Xing, Z. R.; Fu, J. H.; Chen, S.; Gao, J. Y.; Zhao, R. Q.; Liu, J. Perspective on gallium-based room temperature liquid metal batteries. *Front Energy* **2022**, *16* (1), 23−48.

(30) Zhang, Y. Y.; Guo, Z. Z.; Zhu, H. R.; Xing, W. K.; Tao, P.; Shang, W.; Fu, B. W.; Song, C. Y.; Hong, Y.; Dickey, M. D.; et al. Synthesis of Liquid Gallium@Reduced Graphene Oxide Core-Shell Nanoparticles with Enhanced Photoacoustic and Photothermal Performance. *J. Am. Chem. Soc.* **2022**, *144* (15), 6779−6790.

(31) Kumar, V. B.; Gedanken, A.; Porat, Z. Facile synthesis of gallium oxide hydroxide by ultrasonic irradiation of molten gallium in water. *Ultrason. Sonochem.* **2015**, *26*, 340−344.

(32) Peng, X.; Yuan, Y.; Gu, D.; Zheng, X.; Li, D.; Wu, L.; Huang, G.; Wang, J.; Pan, F. Unlocking the Power of Magnesium Batteries: Synergistic Effect of InSb-C Composites to Achieve Superior Electrochemical Performance. *Small* **2024**, DOI: 10.1002/smll.202400967.